Proceedings of the ASME 2010 3rd Joint US-European Fluids Engineering Summer Meeting and 8th International Conference on Nanochannels, Microchannels, and Minichannels
FEDSM-ICNMM2010
August 1-5, 2010, Montreal, Canada

FEDSM-ICNMM2010-30667

QUANTIFICATION OF INERTIAL DROPLET COLLISION MIXING RATES IN CONFINED MICROCHANNEL FLOWS USING DIFFERENTIAL FLUORESCENCE MEASUREMENTS

Brian Carroll, Carlos Hidrovo
The University of Texas at Austin
Multiscale Thermal Fluids Laboratory
Austin, TX, US

ABSTRACT
Efficient mixing at the microscale remains a formidable engineering challenge. Recent advancement and proliferation of Lab-on-a-Chip (LOC) and Micro Total Analysis Systems (μTAS) has demanded accelerated development and demonstration of novel micromixers as successful mixing is critical to device performance. Passive techniques such as chaotic advection and shear thinning as well as active methods utilizing electric fields show great promise at meeting these requirements.

A new droplet-based mixing technique currently being developed aims at improving micromixer rates passively by increasing the Reynolds number in the microchannel. High speed gaseous flows with Reynolds numbers from 1 to 300 are used to detach and transport discrete droplets to a collision zone where droplet interaction and subsequent mixing is achieved under highly inertial conditions. The design utilizes variants of the standard T-junction arrangement for both the detachment and collision process. A fluorescing and non-fluorescing droplet pair are brought into contact in a collision zone and allowed to interact with relative velocities in the 0.1 to 5m/s range. Mixing rates are quantified using an optical based measurement technique that examines temporal changes in droplet intensity as mixing progresses. Both the detachment and collision processes are captured using a high speed camera capable of frame rates in excess of 10MHz.

Experimental results are obtained for different collision zone geometry arrangements and microchannel aspect ratios to assess mixing performance. A description and sufficient explanation of the optical measurement techniques used to quantify mixing rates is provided, including limitations and shortcomings of this simplified approach. Analytical models are developed to gain better understanding of the key physical mechanisms driving droplet mixing and experimental results are correlated against this order of magnitude model. Based on these results, recommendations are made for potential design improvements and issues are addressed concerning mixing using two-phase gas/liquids flows.

INTRODUCTION
Fast, efficient mixing at the microscale remains a challenge in the burgeoning field of microfluidics. The laminar flow regime representative of microchannel flows is not conducive to mixing, which is limited by molecular diffusion under these conditions. The turbulent flow regime exploited at the macroscale for fast mixing is difficult and impractical to induce in microfluidic devices due to conflicting length scales and low Reynolds numbers. The success of future LOC and μTAS is dependent upon achieving fast mixing rates. Scientific understanding of chemical reaction mechanisms requires that molecular mixing be faster than the reaction kinetics under investigation. Proteomics is another emerging application for microfluidics that also requires substantial improvement in fluid mixing rates to accurately examine biological assays. As such, there is currently a push from the chemical and biological fields to achieve mixing rates that are on the order of microseconds or less, while still taking advantage of low sample volumes associated with the use of microfluidics.

However, a number of techniques have been successfully implemented that significantly improve mixing rates for microflows. Such methods can be generally categorized as passive and active techniques. A formal review of such mixer technologies is presented by Nguyen [1]. Passive micromixers utilize microchannel geometry (chaotic advection) and stream thinning (hydrodynamic focusing) to improve mixing rates. State of the art devices in this category have achieved mixing times on the order of micro-seconds for femtoliter detection volumes [2] and milliseconds for nanoliter volumes [3]. Active mixers use means external to the device to promote mixing. Although not inclusive, such mixers use lasers [4], electric and or magnetic fields [5], or mechanical agitation [6].

Bulk mixing times in the range of milliseconds to seconds have been achieved using active methods.

Given the wide range of mixing techniques currently employed, no one method completely satisfies all metrics required to meet the current demands of the next generation of μTAS and LOC devices. These metrics include high mixing rates, increased detection sensitivity for downstream components, high throughput, fluid compatibility, and straightforward integration and implementation. Because mixing time is proportional to the square of the characteristic length, reducing the length for diffusion significantly increases the mixing rate for devices driven by molecular diffusion alone. Continual reduction in diffusion length to the nanometer scale, however, also reduces the device throughput and detection volume.

An alternative to existing mixing technologies that potentially satisfies the metrics outlined is an inertial based droplet micromixer, as shown in Figure 1. This system promotes mixing by utilizing the kinetic energy of two approaching droplets. Each droplet is delivered to a collision zone using a gaseous flow where Reynolds numbers in excess of 200 can be achieved with modest pressure drops (< 10psi).

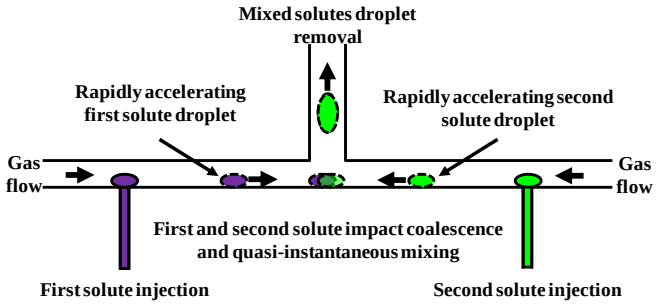

Figure 1. Simplified schematic of an inertial-based droplet micromixer.

A relatively high speed gaseous flow (1 – 20m/s) detaches discrete liquid volumes from two opposing legs of a standard or modified T-junction. Each liquid volume is delivered to a common collision zone through inertial and frictional drag imposed by the gaseous flow. The opposing liquid volumes are allowed to interact under highly inertial conditions and the coalesced and mixed volume is removed through a common exit channel.

Experimental results presented herein show that mixing times on the order of 100s of microseconds for liquid volumes in the 100 picoliter range are achievable using this technique. Mixing rates are increased because the direction of fluid advection and molecular diffusion are aligned unlike parallel flow mixing schemes. The basis of an inertial micromixer is to take advantage of the kinetic energy prior to collision and dissipate this excess energy through viscous dissipation and subsequent mixing within the liquid volume. It is therefore proposed that the droplet mixing time should be inversely proportional to droplet velocity, such that:

$$\tau_{Mix} \sim \frac{1}{V^{\alpha}} \qquad [1]$$

In this relation, α is a positive numbers and V is the relative droplet velocity. Assuming a square dependence, increasing the droplet relative velocity by a factor of two would decrease the mixing time by a factor of four. The droplet velocity cannot be increased indefinitely since droplet coalescence would be usurped by droplet breakup. A droplet coalescence/breakup regime map for confined microflows is not to date well understood in comparison to unconfined droplet interactions.

For the experiment, the mixing rates are quantified using differential fluorescent measurements where an opposing liquid stream is doped with a fluorophore. The fluorophore electrons absorb light at a particular wavelength, are excited to a higher energy level, and quickly return to the ground state by emitting a lower energy wavelength signal. After proper color filtering, this signal is captured digitally at prescribed time intervals and is used for post processing of the mixing event.

On the onset of mixing, there is a large spatial gradient in fluorescent intensity since only one liquid volume is fluorescing. The combined fluid volume intensity becomes uniform as mixing progresses and the total intensity reaches some steady state mean value less than the initially fluorescing single droplet. The total intensity alone, however, does not quantify the progress of mixing. Rather, the standard deviation of intensity computed at discrete time intervals is used to provide a direct measure of mixing.

An order of magnitude analysis is then presented to understand the experimental results. Three different time scales are compared to the actual mixing time: viscous diffusion, molecular diffusion, and convective characteristic. The analysis indicates that the mixing time is of the same order of the viscous diffusion time and is two orders of magnitude greater than the convective time. The molecular diffusion time is significantly greater than the actual mixing time. A successful micromixer must offer substantial improvement over molecular diffusion alone and this device provides mixing rates 10^5 times faster for equivalent volumes.

DEVICE DESIGN

Prior to device microfabrication, the microchannel geometry must first be designed. A number of different collision arrangements were tested that included a standard head-on T-junction, a modified reduced area T-junction (nozzle), and different Y-junction configurations. These arrangements are shown graphically in Figure 2 below.

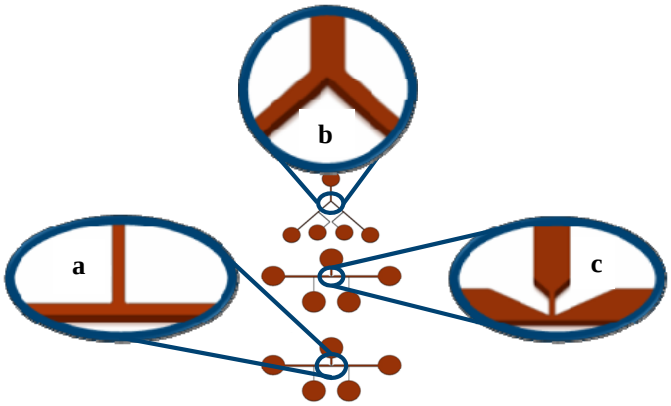

Figure 2. CAD images of the standard T-junction and variations of the standard T-junction: a.) standard T-junction, b.) angled, c.) nozzle.

The channel length leading up to the liquid injection site was designed such that fully developed Poueselli flow is achieved for the range of Reynolds numbers considered. Sufficient length was then added past the injection site such that the droplet growth and detachment process occurs unhindered by downstream channel features and so that the droplet achieves maximum velocity prior to collision. Large plenums of 4mm diameter were added to the air and liquid inlets to facilitate the integration of gas and liquid tubing ports. Channel dimensions range from hydraulic diameters between 50 to 80μm. The depth of the microchannel was held constant in the range of 50μm. The common exhaust channel width ranged from 0.5, 1, and 2 times the individual transport channel width.

DEVICE FABRICATION

The microfluidic device was fabricated with PDMS using soft lithography techniques. The process flow shown in Figure 3 below depicts the major fabrication steps.

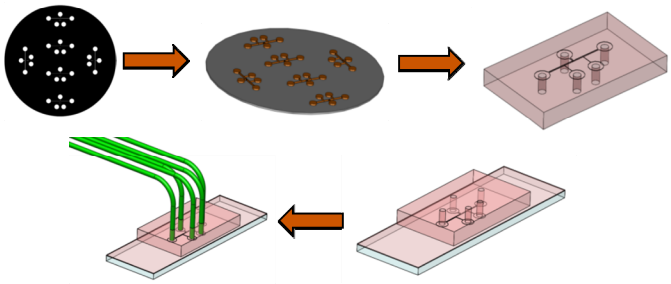

Figure 3. Process flow for PDMS soft lithography: mask design, photolithography, molding, bonding, fluid and gas port integration.

The microfabrication process involved creating a negative mold of the microchannel geometry on a silicon substrate. A standard 4" diameter, 500μm thick silicon wafer was used. The wafer was cleaned and prepared using standard procedures. A negative near UV resist (SU8-2050 MicroChem Corp.) was spin coated onto the wafer to a thickness dictated by the microchannel depth. The coated coated wafer was then baked to remove the solvents in the resist. Once the resist is hardened, the wafer was placed in a Karl Suss MA6 mask aligner and exposed to 392nm radiation through a mask containing the microchannel image. Since the smallest feature size on the microchannel was 20μm, a photo-plotted, 7mil film mask was used as an alternative to a chromium mask. The exposed wafer is then developed using the appropriate developer solution and baked at the prescribed temperature and duration.

Once the negative microchannel mold was complete, the PDMS solution was prepared. Sylgard 184 silicone elastomer base was mixed with a curing agent at a 10 to 1 weight ratio. The wafer was treated with trichlorosilane to render the silicon surface hydrophobic prior to pouring the PDMS. Once the PDMS solution was poured onto silicon and SU8 mold, the assembly was placed in a vacuum desiccators to promote solvent vaporization and air bubble removal. The assembly was then placed on a hot plate in ambient surroundings and baked at 95^{o}C for approximately 3-6 hours. Once fully cured, the PDMS was peeled from the silicon substrate.

The available real estate on a 4" silicon wafer allows a number of devices to be created in a single soft lithography process. Each device is cut from the PDMS in a rectangular shape and prepared for fluid and gas porting. A 2mm diameter belt-hole puncher was used to core the PDMS device at each gas and fluid inlet. The core was then removed using tweezers. Each device was then cleaned with methanol and prepared for bonding.

A 1"x3" standard microscope slide was spin coated with a ~5μm thick layer of PDMS. The glass slide provides a rigid substrate to bond each device to and promotes light transmission for inverted microscope visualization. Each device and PDMS-coated glass slide was placed in a Harrick Plasma cleaning machine. A flow of oxygen was ionized using the integrated RF generator which briefly renders the PDMS surface hydrophilic. Each device was then bonded to a glass slide and baked at 95^{o}C for 8 hours to improve bond strength. The finished device is then checked for dimensional integrity using a microscope and checked for leaks using a pressure source and flow meter.

EXPERIMENTAL SETUP

The experimental setup used to investigate the droplet mixing process in a PDMS microchannel required monitoring and controlling gas and liquid flow rates, channel pressure drop, and inlet temperature and pressure. A host of transducers and data acquisition equipment was employed for this purpose and interfaced via LabView. Droplet growth, detachment, and mixing were visualized using a high speed CMOS camera

(Vision Research Phantom V7.1) and supporting software. The imaging sensor is 800x600 pixels with a square pixel dimension of 21µm. Dry, filtered supply air and distilled water were used for the continuous and dispersed phases, respectively. A schematic of the setup is shown in Figure 4.

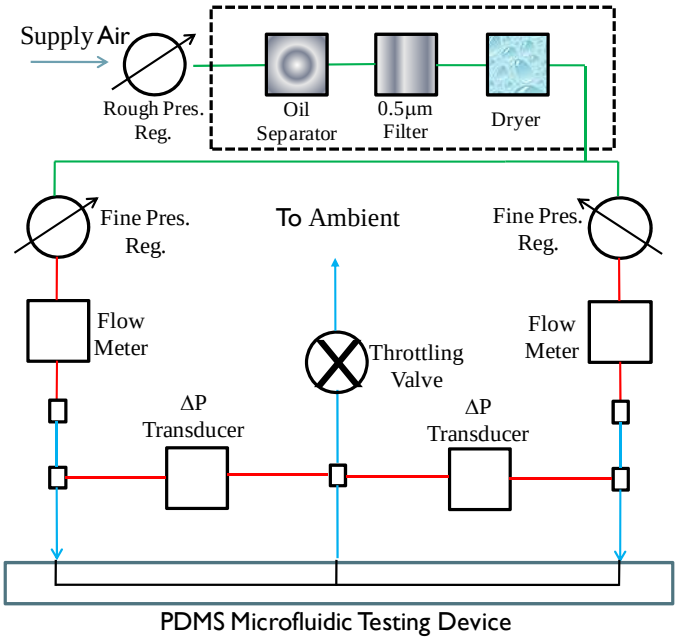

Figure 4. Schematic of experimental setup used for testing droplet detachment and mixing.

Gas inlet pressures were regulated using Omega I/P 710 pressure regulators. Prior to integration, the regulator was calibrated such that the current pressure relationship was established. Once integrated, the regulator was powered using an Agilent 6627A DC power supply and current was inferred using a shunt resistor with the resulting voltage measured using an Agilent 34970A data logger.

Gas flow rates were measured and recorded using a Sensirion ASL 1430 gas flow meter and information was transferred through a RS232 connection. This particular meter uses an internal heat transfer element and differential temperature sensor to measure the flow capacitance. The software then converts, displays, and records this measurement in standard cubic centimeters per minute (SCCM) of N_2. Since the flow meter sits immediately downstream of the pressure regulator, the regulator pressure is used in conjunction with the constant pressure specific heat ratio of N_2 to air to convert the displayed flow rate measurement to actual air flow rate.

Pressure drop across the channel was measured using a Validyne P855-D differential pressure transducer. The high pressure side was connected at the device inlet and low pressure side was connected at the device outlet. The transducer produces a voltage signal in response to the pressure difference acting across the low and high end. The voltage was measured using the Agilent data logger and instrument calibration data was used to convert the signal into a pressure differential.

Liquid was introduced into the device using a Harvard Apparatus PHD2000 syringe pump. The pump is capable of providing constant volume displacements at rates less than 1µl/hr. High dimensional tolerance Hamilton glass syringes were used with the pump and liquid was delivered to the microchannel using 1/16" OD PEEK tubing. Since liquid flow rate measurements were not critical in this experiment, the actual liquid flow rate was determined based entirely on the syringe pump displacement rate.

A Nikon Eclipse TI-U inverted microscope was used visualize the droplet dynamics. The high speed camera was connected to one of the microscope ports to record the mixing process. The camera is capable of frame rates in excess of 100,000 pps, thereby providing the ability to view the droplet growth, detachment, entrainment, and collision events in great detail. The optical diagnostics used to measure the mixing events required a set an optical assembly that includes a beamsplitter and filters. The filters remove particular wavelengths such that only a specific wavelength range is transmitted to the objective and to the high speed camera. The specific wavelength to the objective and to the camera is determined by the fluorophore selected. For this experiment, a green filter and red filter are required. The optical assembly train is shown the in Figure 5 below.

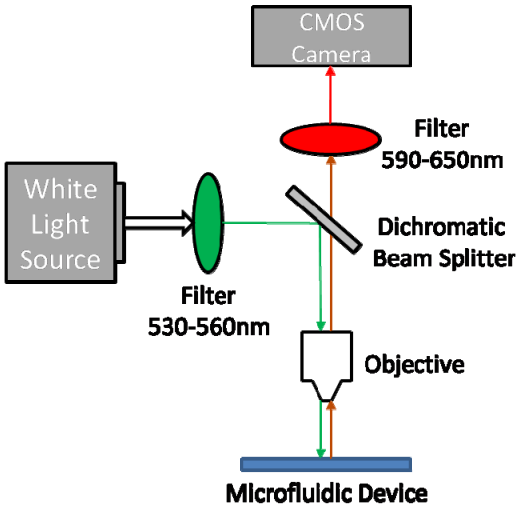

Figure 5. Schematic of optical train used for fluorescent measurements

Image information is sent to a dedicated computer through an Ethernet cable. Resulting images were then processed using the MatLab Image Processing toolbox. Single images were used to determine droplet geometric characteristics for a range of Reynolds numbers considered. Multi-layered images that

capture the mixing events were used for the statistical treatment mixing rates.

OPTICAL DIAGNOSTICS

Quantification of mixing in microfluidic devices requires different techniques from those used at the macroscale. The small volumes in consideration and relatively fast time scales make optical diagnostics the obvious choice. Within this framework a number of different strategies have been described in the literature in great detail. The techniques range from statistical treatment of some received signal [7], typically a fluorophore emission signal, to power spectrum analysis [8]. Such methods are not actual physical measurements of the extent of molecular diffusion but rather statistical treatments of the observed distribution of a tracer dye. It has also been noted that the utilization of fluorophore emission statistics for inferring mixing are sensitive to the orientation of the fluids to the optical plane [9]. Strategies do exist for measuring the extent of actual molecular diffusion using tracer dyes. These rely on monitoring the UV adsorption as an indication of the local ph level in a fluid stream which is representative of intermolecular diffusion [10].

The transient, discrete nature of droplet mixing makes quantifying mixing rates not straight forward. There is no steady stream flow where a fully mixed channel position downstream can clearly be identified and the mixing time can be inferred based on required channel length and bulk fluid velocity. Use of ph measurements requires known droplet volumes prior to mixing such that the change UV adsorption signal is known ahead of time for fully mixed conditions. Presented here is a simple and robust method for quantifying mixing based on the statistical treatment of a fluorophore signal. The goal of this work is to understand how droplet velocity prior to collision influences the mixing process and even though these measurements are not true measures of intermolecular diffusion, this strategy does provide an easy and straightforward way to directly compare different flow conditions, namely the droplet Reynolds number.

The fluorophore selected for this purpose was Rhodamine 610 (Rhodamine B) and was obtained from Exciton. The dye is excited using a source wavelength near 550nm and emits near 590nm. Additionally, this dye has a higher quantum efficiency compared to Rhodamine 6G and Fluorescein [11].

To illustrate this procedure, two droplets are allowed to interact under relatively “slow” velocities (~0.5 m/s) in the angled collision geometry. This is shown in Figure 6 below. The water droplet on the left is doped with Rhodamine B at a concentration of 0.38g/l. The droplet on the right is pure water. The sequence of raw images shows the mixing process. Next to each raw image is a binary image (ones and zeros) that is used to identify the region of interest. Any region with a pixel value of 1 is used for statistics and any region with a pixel value of 0 is not used. The plot in Figure 7 shows the normalized average intensity and standard deviation for each image. The total time is 25ms for a total of 250 images (100μs interval).

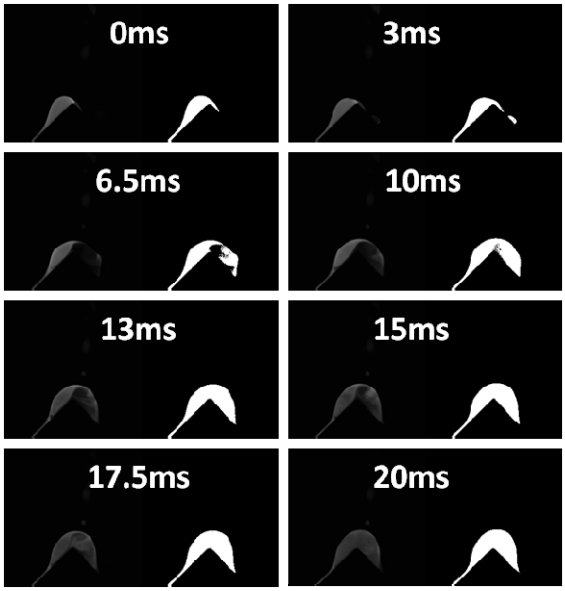

Figure 6. Series of experimental droplet mixing images used to describe the optical diagnostic procedure. The binary images to the left of each raw image identify the region of interest used in the mixing statistics.

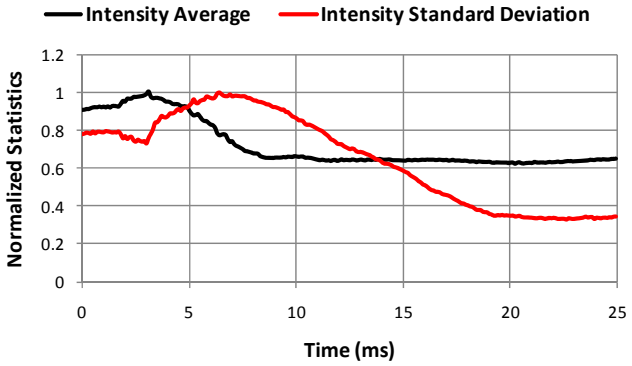

Figure 7. Plot showing how the average intensity and standard deviation change with time for the mixing event shown in Figure 6. Mixing is assumed complete when the standard deviation reaches a minimum.

It is important to note that the average intensity is constant once the binary image includes both droplets. Before the droplets interact, identifying the non-fluorescing droplet is not possible. The time of maximum standard deviation occurs near the onset of constant average intensity. At this time, both droplets are now considered in the statistics. Notice that the standard deviation never achieves zero. This is due to the lensing effect near the droplet boundary. The curvature of the droplet surface refracts the emitted light and locally changes the intensity received by the camera. The mixing time can be

inferred when the standard deviation reaches a minimum and no longer changes with time. This occurs at approximately 20ms with the total mixing time of 12ms.

EXPERIMENTAL RESULTS

Prior to conducting droplet mixing experiments, droplet detachment tests were carried out to understand how droplet geometric characteristics change with the continuous air flow. It is anticipated that as the air flow rate is increased, or more importantly the air Reynolds number, the detached droplet volume should decrease. A microfluidic device, with channel dimensions of 100μmx50μm, was used for this experiment. The air Reynolds number was adjusted from 30 to 130 and the detachment process was captured using the high speed camera. The images were then processed using Matlab and detached droplet height and length were recorded. The results are shown physically in Figure 8 and graphically in Figure 9 where the droplet height and length are scaled according to the channel hydraulic diameter (67μm).

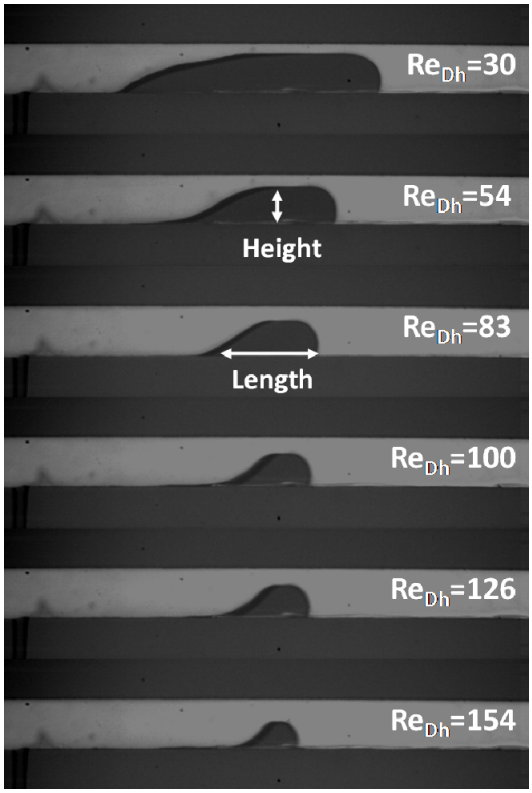

Figure 8. High speed camera images showing how detached droplet size changes with air Reynolds number.

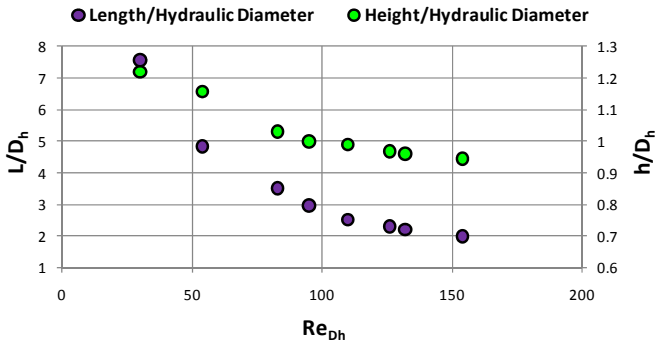

Figure 9. Plot showing how detached droplet length and height decrease with increasing air Reynolds number. Both length and height have been scaled by the channel hydraulic diameter.

The data shows that both droplet height and length decrease with Reynolds number, as expected. If a droplet volume is estimated based on the height, length, and channel depth, such that:

$$V_{Droplet} \sim hLd \qquad [2]$$

A characteristic droplet length scale can be determined as:

$$L_{ch} \sim V_{Droplet}^{1/3} \qquad [3]$$

The plot in Figure 10 shows the dependence of this characteristic length, scaled by the hydraulic diameter, on air Reynolds number. By taking the logarithm of both quantities, a linear fit is observed with a slope of -1/3. This indicates that droplet volume is inversely proportional to the air Reynolds number.

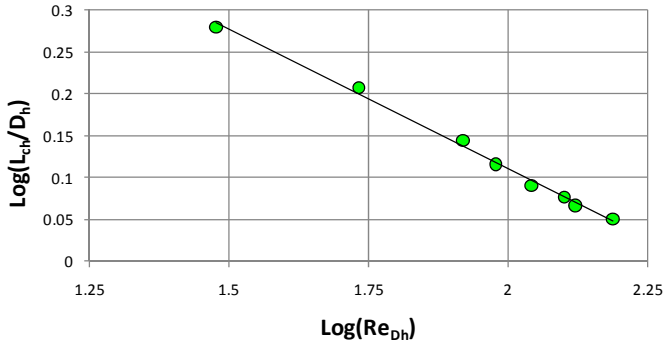

Figure 10. Plot showing how the detached droplet characteristic length changes with air Reynolds number. When the logarithms of both quantities are taken, a linear with slope -1/3 is observed.

Knowing how the characteristic droplet length changes with air Reynolds number is prerequisite for droplet mixing. For purely diffusion driven mixing, a characteristic molecular

diffusion time is proportional to the square of the characteristic length scale, such that:

$$\tau_{Diffusion} \sim \frac{L_{ch}^2}{D} \qquad [4]$$

In this relation, D is the species diffusion coefficient. For Rhodamine B in water, D is approximately $3.4 \times 10^{-11} m^2/s$. This implies that under purely diffusion driven mixing and using an assumed length scale of 70μm, the diffusion time would be approximately 130s. It is proposed, however, that mixing under inertial conditions should significantly decrease the mixing time by orders of magnitude. To achieve mixing times on the microsecond scale, 6 orders of magnitude reduction in total mixing time is required. The detachment results showed that the characteristic droplet length scale decreases with air Reynolds number. Increasing the air Reynolds number also increases the detached droplet velocity. Thus, the air Reynolds number plays a crucial role reducing the droplet size and increasing the droplet velocity, both of which should facilitate decreased droplet mixing times.

To verify the dependence of mixing time versus air flow rate, the channel geometries depicted in Figure 2 were exercised using the optical diagnostic procedure previously outlined. Results indicate that channel geometry significantly influences the mixing time, as shown in Figure 11 below. The mixing rate is maximized using the nozzle geometry since the air flow and droplet is accelerated prior to the collision due to the reduced flow area. The standard T-junction arrangement suffered from droplet deceleration as a result of the abrupt change in direction. The angled geometry showed substantial improvement over the standard T-junction as droplet deceleration was minimized during the approach to the collision zone. However, the relative velocity upon collision is reduced resulting in a decrease in the mixing rate as compared to the head on, nozzle geometry.

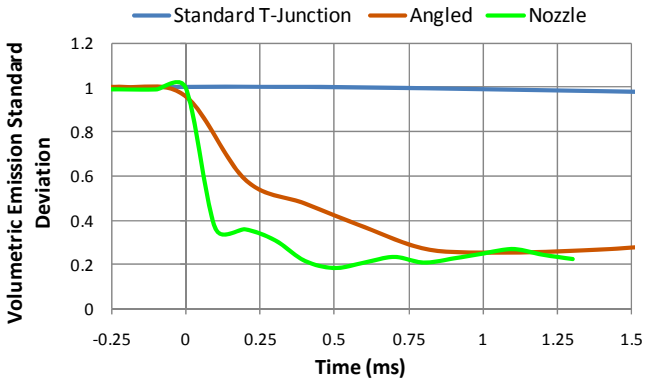

Figure 11. Mixing results for the three channel geometries and an air Reynolds number of 168.

Based on the preliminary channel geometry mixing results, the nozzle geometry was selected for more substantial testing. The air Reynolds number during the tests was varied from 83 to 168. The series of images in Figure 12 shows droplet collision and mixing for an air Reynolds number of 156. The following plot in Figure 13 summarizes the average mixing statistics for four different air Reynolds numbers based on the channel hydraulic diameter.

Figure 12. Series of high speed images depicting the collision and mixing process in the nozzle geometry.

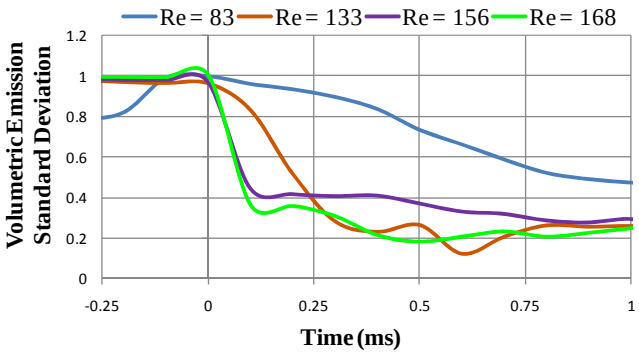

Figure 13. Plot showing how the fluorescent intensity standard deviation changes with time. Mixing is assumed complete when the standard deviation is minimized.

This data can further be reduced by extracting the final mixing time for each Reynolds number considered. The final mixing time was assumed to occur at the minimum of the standard deviation of the fluorescent signal. This is shown below in Figure 14.

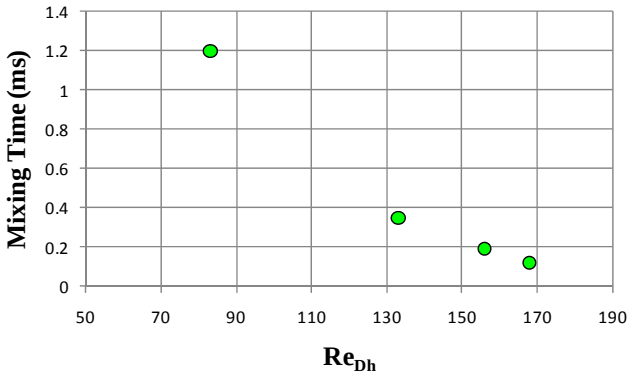

Figure 14. Plot showing how droplet mixing time decreases with air Reynolds number.

The case can thus be made the mixing time is inversely proportional to air Reynolds number, such that:

$$\tau_{Mix} \sim \frac{1}{\mathrm{Re}_{Dh}^{\alpha}} \qquad [5]$$

In this relation, α is some positive number. It is more correct, however, to use a Reynolds number based on the droplet as opposed to the continuous flow. If the assumption is made that droplet velocity prior to impact is equal to the average air velocity (a poor assumption considering the viscous stresses present at the liquid wall interface), the droplet Reynolds number can be formulated as follows:

$$\mathrm{Re}_{Droplet} = \frac{V_{Droplet} L_{ch}}{\nu_{Droplet}} \qquad [6]$$

$$\mathrm{Re}_{Droplet} = \frac{V_{Air} L_{ch}}{\nu_{Droplet}} = \mathrm{Re}_{Dh} \frac{L_{ch}}{D_h} \frac{\nu_{Air}}{\nu_{Droplet}} \qquad [7]$$

$$\mathrm{Re}_{Droplet} = \mathrm{Re}_{Dh} L_{ch}^{*} \nu^{*} \qquad [8]$$

The characteristic droplet length scale at collision can be approximated using the detachment results previously described. These results indicated an inverse relation to air Reynolds number. Applying this result to the droplet Reynolds number yields:

$$\mathrm{Re}_{Droplet} = \mathrm{Re}_{Dh} \mathrm{Re}_{Dh}^{-1/3} \nu^{*} = \mathrm{Re}_{Dh}^{2/3} \nu^{*} \qquad [9]$$

The plot in Figure 15 shows how mixing time varies with droplet Reynolds number.

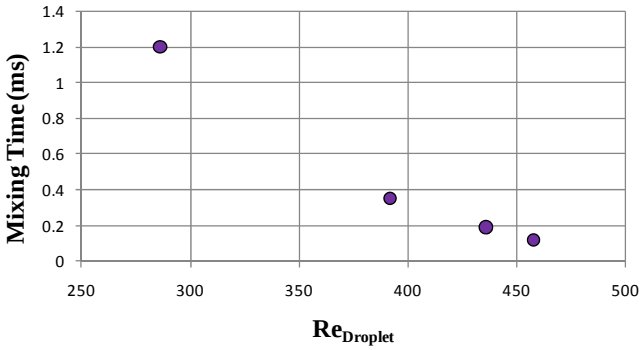

Figure 15. Plot showing how droplet mixing time decreases with droplet Reynolds number.

Similar behavior is observed for mixing time versus droplet Reynolds number as compared to air Reynolds number, but the rate of decrease in mixing time is nearly an order of magnitude greater for the air Reynolds number.

RESULTS DISCUSSION

To date, no verified models for droplet mixing exist for inertial collisions. Insight can be gained, however, by considering an order of magnitude analysis of the momentum and energy equations. It is proposed that mixing under these conditions is facilitated by droplet inertia prior to collision and thus the inertia terms in the momentum equation should be present. Gravity can be neglected due to the large surface area to volume ratio indicative of microflows. Pressure may or may not be significant but, as a first approximation, its contribution should be small. Therefore, the momentum reduces to a balance between inertia and viscous stress. From an order of magnitude perspective, this is shown as follows:

$$\frac{V_{Droplet}^2}{L_{ch}} \sim \nu_{Droplet} \frac{V_{Droplet}}{L_{ch}^2} \qquad [10]$$

This relation implies that the droplet Reynolds number should be of order 1:

$$\mathrm{Re}_{Droplet} \frac{V_{Droplet}}{L_{ch}^2} \sim \frac{V_{Droplet}}{L_{ch}^2} \qquad [11]$$

$$\mathrm{Re}_{Droplet} \sim 1 \qquad [12]$$

This relation clearly does not hold since the droplet Reynolds number is of order 100. Another force balance to consider is inertia to surface tension. This can be written as follows:

$$\rho \frac{V_{Droplet}^2}{L_{ch}} \sim \frac{\sigma V_{Droplet}}{L_{ch}^3} \qquad [13]$$

In this relation, σ is the surface tension of the liquid droplet. This equation can be rearranged and cast in terms of the droplet Reynolds number and Capillary number as follows:

$$\frac{\rho V_{Droplet} L_{ch}}{\mu_{Droplet}} \sim \frac{\sigma}{\mu_{Droplet} L_{ch}} \quad [14]$$

$$\mathrm{Re}_{Droplet} \sim \frac{1}{Ca} \quad [15]$$

$$\mathrm{Re}_{Droplet}\, Ca \sim 1 \quad [16]$$

The capillary number for these experiments is of order 10^{-9} meaning that this relation does not hold as well. Focusing attention to energy considerations, a global energy balance states that the kinetic surface energy prior to collision must equal the kinetic and surface energy following the collision plus any energy dissipated. Assuming that energy is dissipated through viscous dissipation, a global energy balance can be written as:

$$\left(\frac{1}{2}m_1 V_1^2 + \frac{1}{2}m_2 V_2^2 + \sigma L_{ch,1}^2 + \sigma L_{ch,2}^2\right)_{Before} = \left(\frac{1}{2}m_{12} V_{12}^2 + \sigma L_{ch,12}^2\right)_{After} + \mu \frac{V_{rel}^2}{L_{rel}^2} L_{ch,12}^3 \tau_{ch} \quad [17]$$

Using numbers that are representative of the experimental data, the ratio of kinetic energy to surface energy is approximately 100. Assuming that the surface energy can be neglected relative to kinetic energy and assuming that the droplet is brought to rest following collision (completely inelastic collision), the energy balance can be rearranged to find the viscous diffusion time:

$$\tau_{VisDiff} \sim \frac{L_{ch}^2}{\nu} \quad [18]$$

In addition to the viscous diffusion time, two additional characteristics times can be formulated. These are the molecular diffusion time and convective time. Each is written as follows:

$$\tau_{MolDiff} = \frac{L_{ch}^2}{D} \quad [19]$$

$$\tau_{Conv} \sim \frac{L_{ch}}{V} \quad [20]$$

In these relations, D is the diffusion coefficient and V is some representative velocity. Comparing these time scales to the actual mixing time measured from the experiments shows that $\tau_{Conv} < \tau_{VisDiff} < t_{mixing} << \tau_{MolDiff}$. The magnitude of these scales makes sense intuitively since complete mixing cannot occur until material has been convected across the characteristic length. Furthermore, the kinetic energy cannot be dissipated until fluid advection is complete. The fact that the characteristic time for molecular diffusion is much greater than the measured mixing time is a direct consequence of mixing under inertial conditions. If the mixing time was on the same order as the molecular diffusion, there would be no advantage of using the mixer and all potential would be lost.

The plot in Figure 16 shows the ratios of the actual mixing time to the aforementioned characteristic time scales versus droplet Reynolds number. As before, the characteristic length scale was extracted from the droplet detachment results.

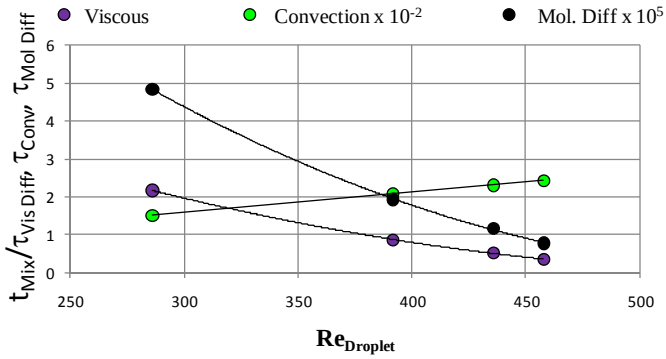

Figure 16. Plot showing the ratio of actual mixing time to the characteristic viscous diffusion, convective, and molecular diffusion time scales versus droplet Reynolds number. The convective time and molecular diffusion time has been scaled by 10^{-2} and 10^{5}, respectively.

An important feature of these results that the ratio of mixing time to viscous diffusion is of the same order throughout the range considered and decreases as $\mathrm{Re}_{Droplet}^{-2}$. The ratio of mixing time to convection time increases linearly with $\mathrm{Re}_{Droplet}$ implying that mixing cannot keep up with fluid advection.

CONCLUSION

This paper describes an experimental investigation of droplet mixing in a confined microchannel flow under inertial conditions. An inertial-based droplet micromixer is illustrated and explained. This micromixer potentially benefits from increased droplet mixing rates for picoliter volumes by using the kinetic energy prior to collision to facilitate volumetric mixing. Mixing times near 200ms have been achieved. The mixing rates were quantified using optical diagnostics of temporally changing fluorescent intensity. Rhodamine 610

chloride (Rhodamine B) diluted with water was used as a fluorophore and allowed to interact with a non-fluorescing droplet in a collision zone. The collision and subsequent mixing is captured using a high speed camera. The collection of images displays spatial changes intensity during mixing due to changes in fluorophore concentration. The images are statistically analyzed to arrive at an estimated mixing rate.

An explanation of the experimental results is provided that attempts to understand how mixing time is affected by the relative droplet velocities. An order of magnitude analysis is made that shows the mixing time scale is on the order of the characteristic viscous diffusion time. The second relevant time scale is the convective time which characterizes the time required to move bulk material some characteristic distance. The actual mixing time is also compared to the molecular diffusion time scale. A successful micromixer must exhibit mixing rates orders of magnitude faster than the time required for molecular diffusion. The mixing results presented herein are 10^5 times faster than that of species diffusion alone.

Significantly more work is required to fully understand droplet dynamics upon collision in confined microflows. The literature contains ample theoretical, numerical, and experimental work on droplet interactions in unconfined scenarios [12, 13, 14, 15, 16]. Results show specific regimes of coalescence based on the ratio of droplet inertia to surface tension. The presence of microchannel walls changes the physics of the collision process but parallelisms must be present. Since the inertial droplet micromixer requires coalescence for mixing to proceed, there is an upper limit on the relative kinetic energy of interacting droplets for mixing to occur. The experimental results do show that mixing rates are proportional to the relative velocity raised to some power. The droplet detachment results show that droplet volume, and hence characteristic length, is inversely proportional to the continuous phase velocity. Droplet velocity upon collision is also directly proportional to the continuous phase velocity. The interrelation of these variables needs to be clarified. More mixing experiments at higher and lower droplet Reynolds numbers are required to fully predict the expected rate of mixing versus both discrete and continuous phase velocity.

Additionally, the optical diagnostic process needs improvement. The inability to locate the non-fluorescing droplet prior to and during the initial stages of the mixing event reduces the accuracy of the statistical strategy. The strategy is based on the volumetric emitted signal of dye concentration and therefore requires tracking of the total liquid volume. A possible solution is to use two fluorescing droplets of significantly different dye concentrations. This will enable locating both droplets and also provide a direct means of measuring the relative velocity upon impact, thus allowing a calculation of droplet Reynolds number. Increasing the fluorescent signal would also improve the accuracy of the approach. Experimental observation has shown that increasing the dye concentration does not necessarily increase the emitted intensity and can actual reduce the signal significantly due to self quenching. Increasing the dye concentration increases fluorophore to fluorophore collisions. These collisions are inelastic and reduce the energy level of the fluorophore before a photon is emitted. Characterization of the emitted intensity versus dye concentration is needed to ensure that the emitted intensity is monotonic across the concentrations considered. If two different concentrations yield the same intensity, the outlined optical diagnostic approach would be flawed since it is based on the statistics of the received fluorescent signal.

Work is also required on optimizing the collision geometry. The preliminary results of T-junctions variations show improved mixing rates using the nozzle geometry. However, observations of droplet dynamics in collision zone show increased droplet deformation prior to collision due to the reduced flow area. This behavior may make droplet control difficult and negate the improved mixing rates.

REFERENCES

1. N. T. Nguyen, "Micromixers-a review," *Journal of Micromechanics and Microengineering*, 15, 2005
2. D. Hertzog, B. Ivorra, B. Mohammadi, O. Bakajin, J. Santiago, "Optimization of a Microfluidic Mixer for Studying Protein Folding Kinetics," *Analytical Chemistry*, 78, 2006, 4299-4306
3. A. Stroock, S. K. W. Dertinger, A. Ajdari, I. Mezic, H. Stone, G. M. Whitesides, "Chaotic Mixer for Microchannels," *Science*, 295, 647, 2002
4. A. Hellman, K. R. Rau, H. H. Yoo, S. Bae, J. F. Palmer, K. S. Phillips, N. L. Allbritton, V. Venugopalan, "Laser-Induced Mixing in Microfluidic Channels," *Analytical Chemistry*, 79, 2007, 4484-4492
5. F. Bottausci, C. Cardonne, C. Meinhart, I. Mezic, "An Ultrashort Mixing Length Micromixer: The Shear Superposition Micromixer," *Lab on a Chip*, 7, 2007, 396-398
6. B. Cola, D. K. Schaffer, T. S. Fisher, M. A. Stremler, "A Pulsed Souce-Sink Fluid Mixing Device," *Journal of Microelectromechanical Systems*, 15, 1, 2006
7. R. H. Liu, M. A. Stremler, K. V. Sharp, M. G. Olsen, J. G. Santiago, R. J. Adrian, H. Aref, D. J. Beebe, "Passive Mixing in a Three-Dimensional Serpentine Microchannel," *Journal of Microelectromechanical Systems*, 9, 2, 2000
8. M. H. Oddy, J. G. Santiago, J. C. Mikkelsen, "Electrokinetic Instability Micromixing," *Analytical Chemistry*, 73, 2001
9. M. Munson, P. Yager, "Simple Qualitative Optical Method for Monitoring the Extent of Mixing Applied to a Novel Microfluidic Mixer," *Analytica Chimica Acta*, 507, 2004
10. W. Ehrfeld, K. Golbig, V. Hessel, H. Lowe, T. Richter, "Characterization of Mixing in Micromixers by a Test

Reaction: Single Mixing Units and Mixer Arrays," *Industrial and Engineering Chemistry Research*, 38, 1999
11. C. Arcoumanis, J. J. McGuirk, J. M. L. M Palma, "On the Use of Fluorescent Dyes for Concentration Measurements in Water Flows," *Experiments in Fluids*, 9, 1990
12. C. H. Wang, K. L. Pan, S. Y. Fu, W. C. Huang, J. Y. Yang, "An Experimental Investigation of the Coalescent Behaviors of Colliding Droplets," *Journal of Mechanics*, 23, 4, 2007
13. N. Nikolopoulos, K. S. Nikas, G. Bergeles, "A Numerical Investigation of Central Binary Collision of Droplets," *Computers and Fluids*, 38, 6, 2009, 1191-1202
14. K. L. Pan, C. K. Law, B. Zhou, "Experimental and Mechanistic Description of Merging and Bouncing in Head-On Binary Droplet Collision," *Journal of Applied Physics*, 103, 2008
15. Y. Pan, K. Suga, "Numerical Simulation of Binary Liquid Droplet Collision," *Physics of Fluids*, 17, 2005
16. J. Qian, C. K. Law, "Regimes of Coalescence and Separation in Droplet Collisions," *Journal of Fluid Mechanics*, 331, 1997, 59-80